# Analysis of Dispersion Process of Evaporating Spray Droplets Using Novel Scale Adaptive Simulation Approach coupled to a Langevin Dispersion Model

W.Ahmadi1*, A.Mehdizadeh, A.Sadiki
TUD, Dept of Mechanical Engineering, Institute of Energy and Power Plant Technology, Darmstadt, Germany
ahmadi@ekt.tu-darmstadt.de and mehdizadeh@ekt.tu-darmstadt.de

**Abstract**

In this paper, an advanced scale adaptive simulation approach (SAS) is developed and used to achieve time dependent and three dimensional space resolved simulation of large-scale structures which describe the turbulence dynamics. This features a zonal hybrid URANS-LES strategy that allows to capture needed unsteady flow structures using economical computational costs. In order to quantify the small-scale instantaneous velocity seen by the particle as it appears in the droplet motion equation and its effect on the droplet distribution, three different dispersion models are used. The evaporating droplets are captured using the Lagrangian procedure in which all numerical droplets are tracked by solving their equations of motion that include only the drag and gravitation force. The spray is diluted as the droplet volume fraction has a maximum value of $2.6.10^{-4}$micrometer allowing a full two way coupling. With regard to evaporation, the Uniform Temperature Model is applied. Note that all the assumptions required for the use of the model set are valid in the investigated configuration.

---

## Introduction

In various engineering applications, such as IC engines, gas turbine combustors, industrial furnaces, etc., sprays are characterized by highly unsteady interacting processes, like injection of the liquid fuel, dispersion, evaporation, mixing and combustion. Apart from the injection process, dispersion influences the droplet trajectories that are especially important when evaporation takes place or when temperature and chemical composition of the particles depend on their history. Phenomena, like droplet segregation or inter-droplet interaction that mainly occur in wall-bounded regions and recirculation zones of engine configuration flows, may affect the spray evolution and spray flame propagation. Such phenomena are highly affected by turbulence small scales. To investigate the effects of these phenomena in complex configurations, small scales have to be either resolved or modelled. As DNS is computationally prohibitive, LES is often preferred. However, LES suffers from severe shortcomings in most wall-bounded flows and need alternatives or improvements.

Recognizing the limitations of the classical RANS/URANS and LES and in search for more efficient solution methods for practical applications, the CFD community has recently turned its attention to so called hybrid URANS-LES modeling as an alternative strategy for complex turbulent flows with high Reynolds numbers. The main goal of an LES/URANS hybrid approach is to achieve time dependent and three-dimensional space resolved simulation of large-scale structures which describe the turbulence dynamics. However, this should be obtained by using a mesh density which is typical for URANS or off-wall LES. It is recalled that near-wall URANS also requires fine grid clustering towards the wall, but much coarser than in conventional LES. The basic idea of hybrid approach is therefore, to apply a URANS model in near wall region and an LES model away from the wall. In present investigation the results obtained from standard $k-\epsilon$ model using an unsteady coupling approach for both phases will be presented. Furthermore, an advanced zonal hybrid turbulence model for complex wall bounded shear flows is developed completely based on Reynolds-averaged- Navier-Stokes (RANS) concepts using Rotta's original transport equation (see [1]) for turbulence integral length scale. This model overcomes mathematical and physical inconsistencies of existing hybrid URANS/LES models and is suitable for the LES approach. The model was successfully tested on several flows, including generic and also complex cases. The results first for carrier phase is compared the standard $k-\epsilon$ results.

## Experimental and numerical setup Spray issuing into a co-flowing heated air stream

Simulations of two phase flows represented by a spray which is injected into a co-flowing heated air-stream are presented and discussed in this test case. The objective of these simulations is to assess the ability of the equilibrium uniform temperature evaporation model as well as the different dispersion models, compared in the

*Corresponding author: ahmadi@ekt.tu-darmstadt.de

**Table 1.** Flow conditions for the considered two phase flows

| Cases | Air volume flow rate $(g^3/s)$ | Air mass flow rate (g/s) | Maximum air velocity (m/s) | Air temperature (ï¿½C) | Liquid mass flow rate (g/s) | Liquid temperature at nozzle exit (ï¿½C) |
|---|---|---|---|---|---|---|
| 1 | 0.032 | 29.0 | 18.0 | 80 | 0.00 | 0.0 |
| 2 | 0.032 | 29.0 | 18.0 | 80 | 0.44 | 32.0 |

above test case to successfully predict the mass transfer, vapor and droplet spatial distributions. These numerical investigations are important in order to characterize the interaction regimes between processes that occur during evaporation, namely turbulence and heat transfer. These regimes govern the conditions for the fuel air mixing preparation.

***Spray issuing into a co-flowing heated air stream***

***Configuration***

The configuration under study is the experiments with polydispersed evaporating sprays reported by Sommerfeld et al.[2]. The experimental test case shows an axisymmetric, turbulent, two-phase jet. This configuration is consisted of a pipe with an expansion ratio of three, where heated air is injected through an annulus with $64mm$ outer diameter (see Figure 1). The nozzle holder had a size of $38mm$, and the test section had a diameter of $198mm$. A two-component phase Doppler anemometry (PDA) is used to measure droplet velocities and diameters simultaneously and to discriminate gas-phase tracers from the different size-classes of droplets. Due to its high evaporation rate an isopropanol-alcohol spray liquid was chosen. Measurements were taken for different flow conditions, such as air flow rate, droplet velocities, droplet diameter distribution and liquid flow rate in order to provide a set of reliable date. Measurements are available in six cross-sections downstream for droplets and carrier phase, namely at: $x = 25$, $x = 50$, $x = 100$, $x = 200$, $x = 300$ and $x = 400mm$. This experiment gives a valuable database of polydispersed two-phase flows since initial conditions are detailed for each droplet size class. The initial conditions are given at $3mm$ downstream due to measurement technique limitations.

In order to assess the flow characteristics the first flow considered in the studies was a single phase flow case (i.e. liquid spray is not operated). In Table 1 the air flow conditions for the single phase are summarized . Grid independent solutions were obtained using enough refinements and central differencing scheme. The computational domain for the simulation was represented by a grid having almost $7 * 10^5$ control volume (see Figure 2). The heated air inters the configuration in x-direction the inlet with the constant velocity of $18m/s$ and $80C$.
The simulation is first performed in steady mode with k-$\epsilon$ and the boundary condition for the turbulent kinetic energy was set to $5\%$ of the mean flows inlet velocity. This practice lead to a good convergence behaviour of the SAS-model. After 3000 Iteration in steady mode the simulation was changed to unsteady mode (with $\Delta t = 5 * 10^{-5}$s) and SAS-model was switched on.

For the two-phase flows, the inlet boundary conditions for the carrier phase are given in Table 1. For Validation purpose the measurements were performed $3mm$ downstream for all three velocity components as well as the associated rms values. More details on the test cases are provided by Sommerfeld et al. [2] in the inlet section for all carrier phase variables. 8 different classes of droplet can be generated by the hollow-cone pressure atomizer. These classes are distinguished by the droplet diameter, start velocities, start locations and rms values. the inlet properties for the different classes are given in Table 2. It should be mentioned here that, the mean tangential velocity of the droplet inflow during the simulation were set to zero (not conform to the experimental boundary conditions), since a spray nozzle without swirl was used and, therefore, the measured mean tangential velocity was due to disturbances from the flow at the edge of the nozzle exit. The Table 1 gives the total liquid mass flow rate and the inlet temperature at the nozzle exit. 100000 parcel trajectories are calculated every coupling iteration in order to get statistically reliable results. An increase of parcel number had no influences on the statistical droplets properties.

**Table 2.** Flow conditions for the considered dispersed phase

| z (mm) | flux $(g/m^2/s)$ | size $\mu m$ | $U_{mean}$ (m/s) | $U_{rms}$ (m/s) | $V_{mean}$ (m/s) | $V_{rms}$ (m/s) | $W_{mean}$ (m/s) | $W_{rms}$ (m/s) |
|---|---|---|---|---|---|---|---|---|
| 0 | 88.6 | 18.10 | 7.698 | 3.307 | 0.508 | 1.452 | -0.749 | 1.037 |
| 1 | 214.5 | 20.51 | 10.688 | 3.674 | 2.107 | 0.898 | -0.434 | 0.829 |
| 2 | 952.5 | 28.22 | 14.386 | 3.021 | 5.054 | 1.225 | -0.243 | 0.669 |
| 3 | 3080.7 | 36.54 | 16.017 | 2.442 | 7.785 | 1.248 | -0.120 | 0.586 |
| 4 | 6321.3 | 44.61 | 15.93 | 2.022 | 9.766 | 1.530 | -0.034 | 0.533 |
| 5 | 5664.5 | 47.47 | 14.295 | 2.126 | 8.740 | 3.443 | -0.001 | 0.530 |
| 6 | 973.7 | 37.96 | 10.436 | 2.593 | 6.200 | 4.569 | -0.095 | 0.606 |
| 7 | 95.0 | 27.98 | 6.178 | 2.835 | 2.303 | 3.530 | -0.250 | 0.794 |

***Results and discusions***

It is very important to look first on the gas phase. For the turbulence closure 2 different model are used, the k-$\epsilon$ and the new implemented SAS model in the FASTEST-Solver.

The configuration under study is a high turbulent flow. In addition to the turbulence induced through the inflow the inner and outside shear layer provide some more turbulence intensity. The eddies induced through the shear layer lead to the groth of the turbulent length scale. Figure 4 shows the instantaneous picture of the axial velocity of fluid phase for the SAS (top) and k-$\epsilon$ model (bottom). The turbulent nature of the flow is very well seen by the SAS model, whereas the k-$\epsilon$ model shows a converged solution. A closure look to the SAS picture 4 gives an impact of the captured scales. The big scales are very important for the evolution of the droplet.

The comparision to the experiments are shown in Figure 3, where axial mean velocity (top), axial RMS values of velocity (middle) and radial mean velocity (bottom) of the gas-phase along the test section are confronted with experimental data. Generally the agreement to the experimental data is well for both models regarding the axial velocity. Forthermore one can see that the SAS model is able to predict the radiale component very well compared to the k-$\epsilon$ model, which is normaly very difficult to capture due to its low values. The comparison of the first section regarding the rms values shows that the k-$\epsilon$ model is not able to predict the rms values in this section, whereas the SAS model is able to perform the trend of the rms values in the high unseady area and a satisfactory agreement away from this area. The results are getting better the more one goes away from the pipe inlet.

The rms values of the velocity in x-direction is very well captured by the SAS model. This ensures that the the energy is successfully transferred from the modelled to the resolved part and the spectral distribution improves with time as the process is controlled by the momentum equations and the eddy-viscosity provided by the SAS model. The shown results are provided by 56000 time steps. For the k-$\epsilon$ model an almost steady solution was reached after almost 16000 time steps. Since the resolved rms values of the k-$\epsilon$ model were very low only $1/3$ of the turbulent kinetic energy was taken for comparison to the SAS model. Since there have to be some work done for the coupling of the SAS model to the dispersed phase the following towphase flow simulation are carried out with the K-$\epsilon$ model.

In the following three dispersion models, PLM (Particle Langevin Dispersion model) (see Minier et al. [5]), RWM-Iso (Isotropic Random Walk model) (see Sadiki et al. [6]) and RWM-Aniso (Anisotropic Random Walk model) (see Legg et al. [7]) are used to determine the instantaneous fluid velocity seen by the droplet. For the evaporation the equilibrium evaporation model is implemented and used in combination with above mentioned dispersion models.

First, the capability of the Lagrangian tracking approach is evaluated to capture the dynamic droplet behavior

by comparing the calculated droplet velocities with experimental data. The velocities in axial direction are plotted in Figure 5 as function of radial positions at different axial positions. One observes some differences between experimental and numerical results. In particular, at $x = 300mm$ and $x = 400mm$ the computed droplet axial velocities are about $2m/s$ higher at the centerline than the measured values. However, it is remarkable that the choice of dispersion model does not influence too much the numerical droplet axial velocities. Whereas some advancement are seen by PLM model especially outside of the centerline.

Figure 6 shows the radial droplet velocity at different axial cross sections. It is seen that the effects of the small recerculation zones are reflected in the first two cross sections downstream of the inlet where negative radial velocitiess can be observed. The influence of the drift correction factor (RWM) on the droplet radial velocities is only not seen at the first axial section. The radial mean velocity of the droplets decreases when moving away from the nozzle inlet by the RWM. The RWM-Aniso improve the results, wheras the PLM capture the radial velocity very well. The Comparison of the numerical and experimental results of the radial mean velocities show that the radial position of the spray is not well reproduced at the first two positions downstream of the nozzle. The deviations from the experiment may lie in intial conditions of droplets at the nozzle exit such as the radial velocity and positions which were very difficult to be extracted from the experimental data.

In Figure 7 the radial distribution of the mean droplet diameter is shown at different axial positions (x= 25, 50, 200, 300 and $400mm$) which were close to inlet, center and outlet regions. Due to the evaporation and spreading of the droplets, the mean diameter becomes more uniform when moving away from the inlet nozzle. The droplet diameter decreases while moving downstream of the nozzle exit. At sections of x= 25 and 50 one observes a zero mean diameter (radius > $0.03m$) while including fluctuating diameter for the sections x= 200 and $300mm$. This lies due to the fact that no droplets or very less droplets are registered within the control volumes. This lead in case of less droplets to a fluctuating variable fields of the statistical averaging (see Figure 7 x= 200, 300 and $400mm$).

Th axial mean values (RMS) of the droplet velocity is shown in Figure 8. Based on the results, it can be concluded that the RWM-Iso underpredict the particle fluctuations, which might be due to the fact that the RWM-Iso is not capable to account for anisotropy of the flow induced by shear gradient effects. The RWM-Aniso improves the results to some degree but still some disagreements with experimental data can be observed (see Figure 8 x = $50mm$ and x = $200mm$). For x = $25mm$ the PLM results overpredict the fluctuation, whereas x = $50mm$ and x = $200mm$ are predicted very well. The sections x = $300mm$ and x = $400mm$ are characterized by a fluctuating variable field which is due to wider spreading of droplets by PLM and the statistical averaging.

The radial distribution of the droplet mass flux at different axial positions ($0.025m$, $0.05m$, $0.1m$, $0.2m$, $0.3m$ and $0.4m$ far away from the inlet) are presented in Figure 9. It is well seen, that the concentration of droplets decreases while moving away from the nozzle due to the evaporation. This fact is illustrated by all three dispersion models (RWM, RWM-Aniso and PLM). A comparison between these models reveals that the PLM delivers results much closer to experimental results and especially far away from the nozzle. In the absence of electrostatic and thermophoretic forces, the deposition of small particles depends mainly on particle Stokes number (see [3]). The Stokes number for the particle is defined as the ratio of the particle response time, $\tau_p$, to the turbulence typical Lagrangian time scale $\tau_l$. In the present study this quantity lies in range of $(0, 0.5)$. Therefore the use of dispersion modeling is revealed to be very important for the current configuration as pointed also by [4].

***Summary and Conclusion***

In this study different dispersion models are used in combinations with the uniform temperature evaporation model to investigate the spray and droplet properties under turbulent conditions. The results show that the PLM is able to achieve better results with respect to radial mean velocities, mean diameter and axial mean velocity fluctuations of droplets. So the Simulations have shown that the PLM model agreed very well with the experimental measurement of the droplet mass flux in particular in upper sections. This means that the considering the advanced dispersion models like PLM can help to capture complex dynamics of turbulent flows. Furthermore the results obtained from new hybrid turbulence model for the carrier phase indicate a strong improvement compared to the standard$k - \epsilon$ model. The coupling of the new model with Lagrangien particle tracking method is in progress and the results for particle phase will be addressed in future.

## References

[1] Rotta, J.C., *Turbulente Srtömungen*, Teuber Verlag, Stuttgart (1972).

[2] Sommerfeld M.;Qiu H.-H., *Experimental studies of spray evaporation in turbulent flow*, International Journal of heat and fluid flow,**19, No. 1**, 10–22(13) (1998).

[3] Pope, S. b., (1994): *Lagrangian pdf methods for turbulent flows*.Annu. Rev. Fluid Mech., , **26**, 23–62

[4] P. Fede, O. Simonin, P. Villedieu and K. D. Squires (2006): *Stochastic modeling of the turbulent subgrid fluid*

*velocity along inertial particle trajectories* Proceeding of the Summer Program 2006, Center for Turbulence Research

[5] Minier, J.-P., and Peirano, E., (2001): *The pdf approach to turbulent plydispersed two-phase flows*, Physics Reports, 352, pp. 112-126

[6] Sadiki, A., Chrigui, M., Janicka, J., Maneshkarimi, M.R. (2005): *Modeling and simulation of effects of turbulence on vaporization, mixing and combustion of liquid-fuel sprays.*. Flow Turbul. combust. **75**, 105–130.

[7] Legg, B. J. and Raupach, M. R., (1982): *Makrov-Chain Simulation of Particle Dispersion in Inhomogeneous Flows: the Mean Drift Velocity induced by a Gradient in Eulerian Velocity Variance*, Boundary-Layer Meteorol. 24,3-13

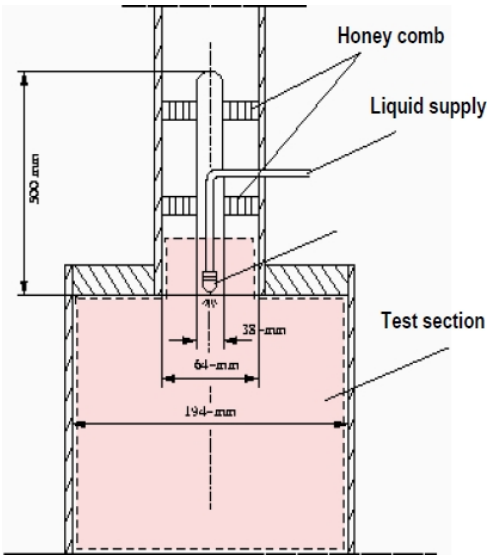


**Figure 1.** Test configuration for spray issuing into a co-flowing heated air-stream

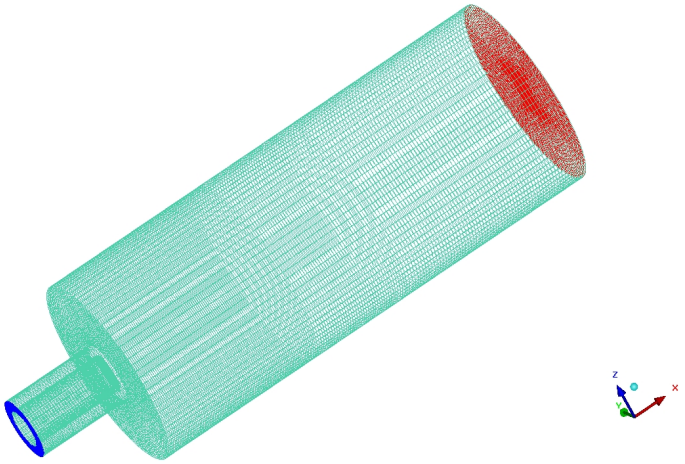

**Figure 2.** Mesh for the test configuration for spray issuing into a co-flowing heated air-stream

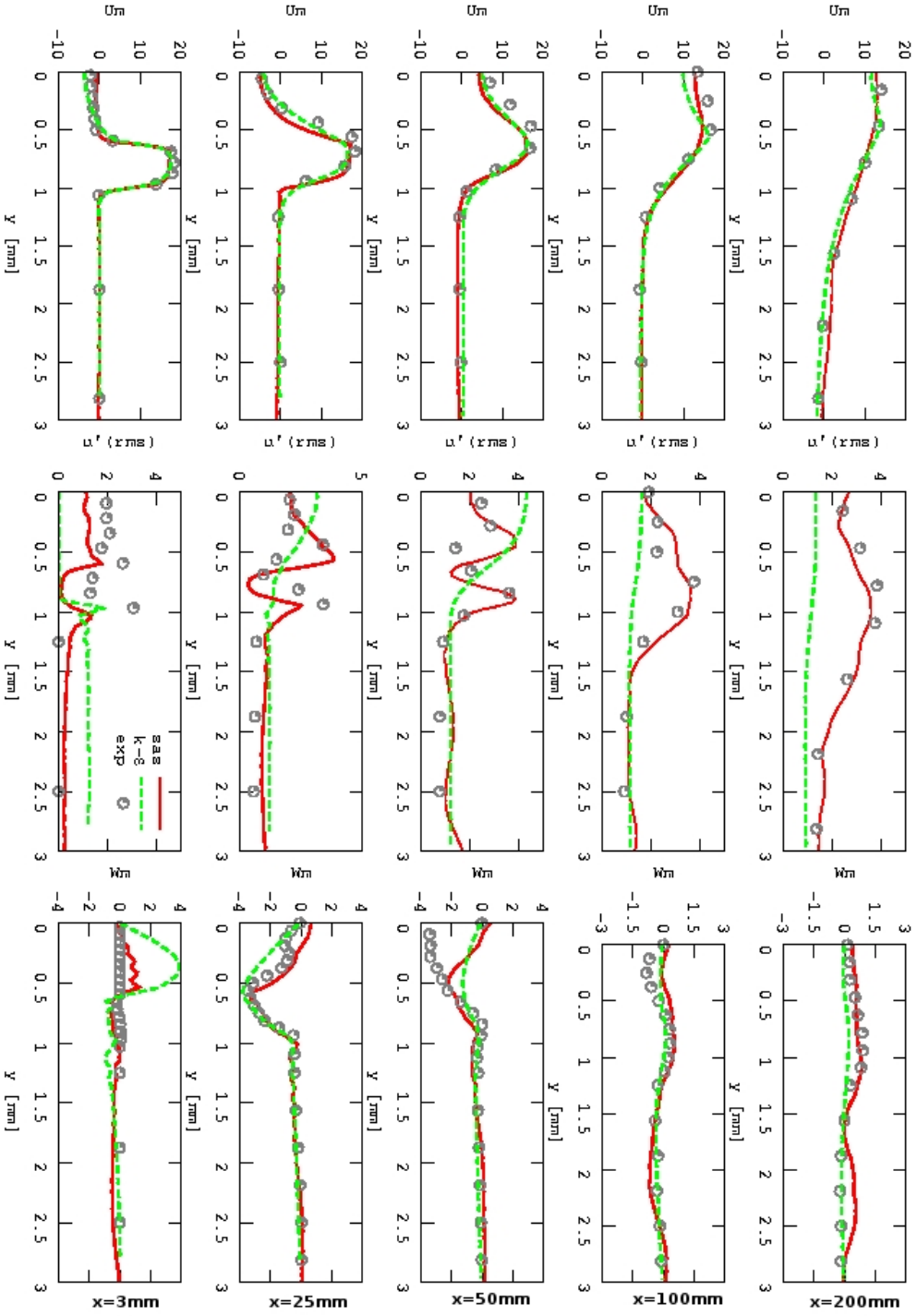


**Figure 3.** Cross sectional distributions of (top) axial mean velocity, (middle) axial RMS values of velocity and (bottom) radial mean velocity of the gas-phase along the test section

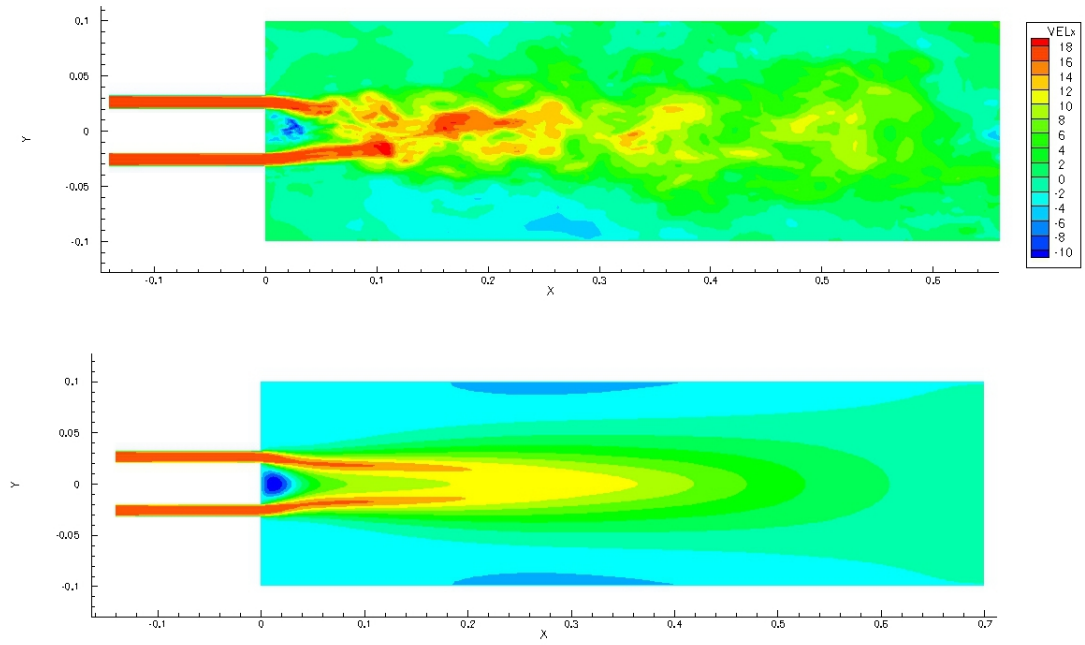


**Figure 4.** Instantaneous picture of the axial velocity of fluid phase for the SAS (top) and k-$\epsilon$ (bottom). two dimensional cut through the symetry axis

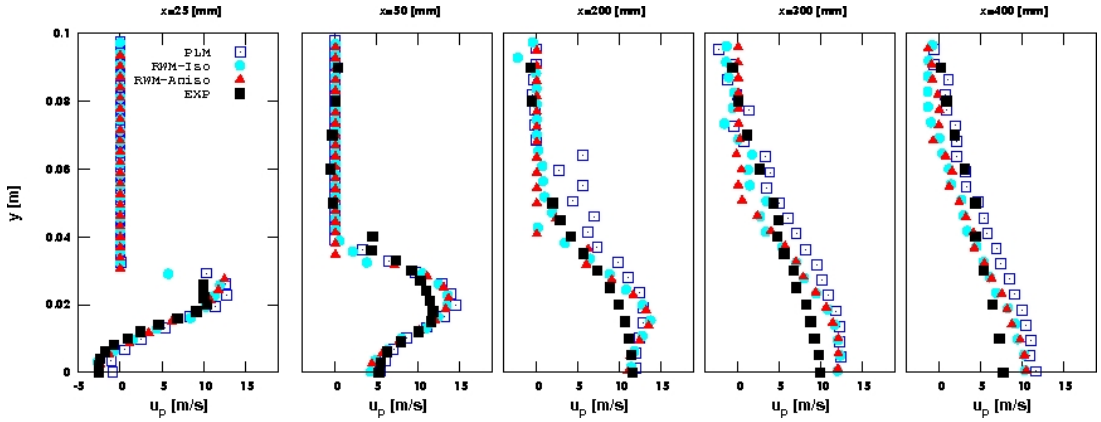


**Figure 5.** Cross-sectional distributions of axial mean velocities of droplets along the test section

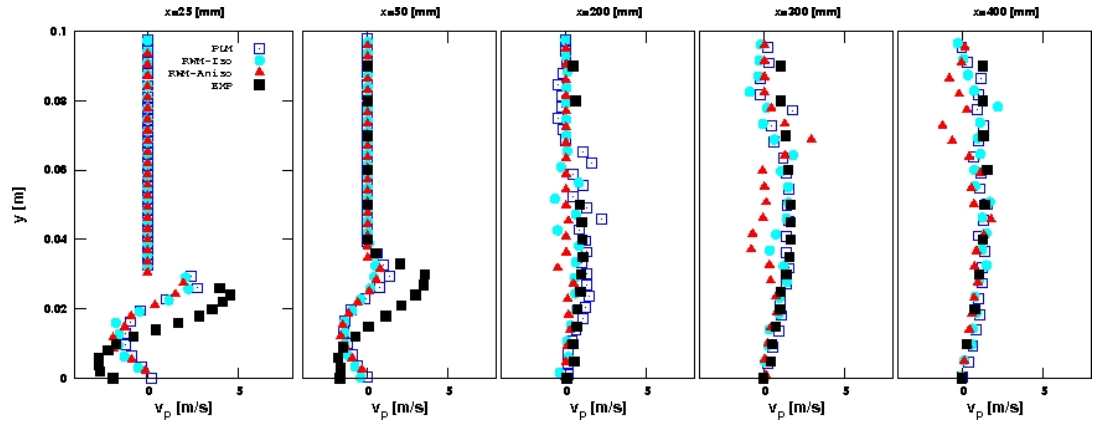


**Figure 6.** Cross-sectional distributions of radial mean velocities of droplets along the test section

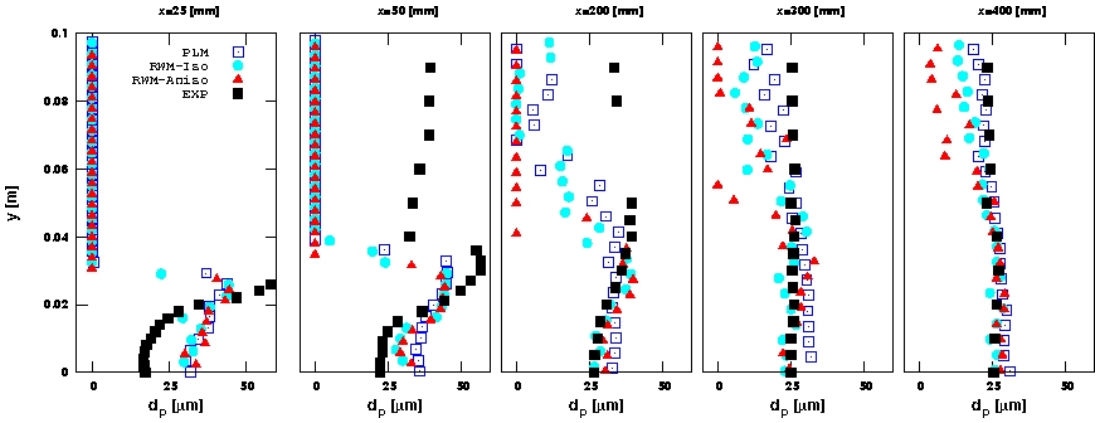


**Figure 7.** Cross-sectional distributions of axial mean diameter of the droplets along the test section

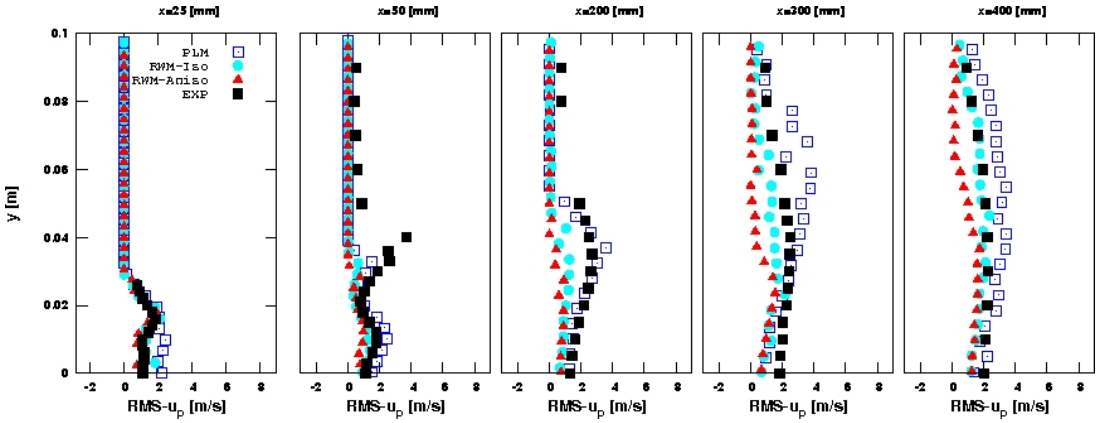


**Figure 8.** Cross-sectional distributions of axial mean velocity fluctuations of droplets along the test section

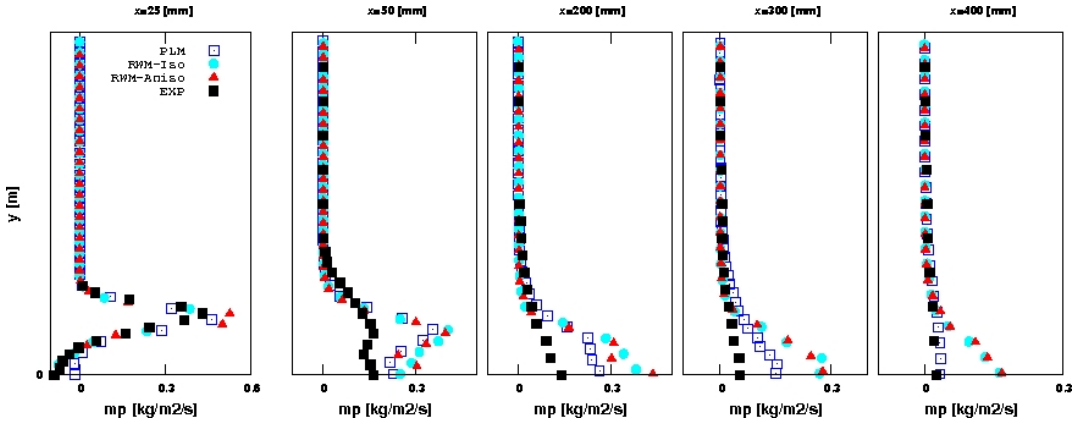


**Figure 9.** Cross-sectional distributions of the droplet-mass flux along the chamber